JOURNAL OF SOLID STATE CHEMISTRY **141,** 323–329 (1998)
ARTICLE NO. SC987926

Synthesis and Characterization of Poly(ethylene Oxide) Nanocomposites of Misfit Layer Chalcogenides

Lourdes Hernán, Julián Morales, and Jesús Santos

Laboratorio de Quimica Inorgánica, Facultad de Ciencias, Universidad de Córdoba, Avenida San Alberto Magno, s/n, E-14004 Córdoba, Spain

Received December 31, 1997; in revised form June 2, 1998; accepted June 15, 1998

Nanocomposites of poly(ethylene oxide) (PEO) and $(PbS)_{1.18}(TiS_2)_2$, a composite misfit layer sulfide were prepared by treating a lithium derivative in aqueous solutions of PEO. Under these conditions, the alkali metal intercalate readily exfoliates and rapidly reflocculates, thus trapping polymer molecules between sulfide layers. In this exfoliation and restacking process, Li^+ ions are partially removed. Powder X-ray, electron diffraction, and IR results are consistent with one layer of helical PEO located at all TiS_2-TiS_2 interfaces and with empty PbS-TiS_2 interfaces. Thermal deintercalation of the new phase is a complex process that occurs at an unusually high temperature; this sugggests strong interactions between the polymer and the host, probably involving the alkali ions and PEO chains. Hydrogen sulfide traces were also detected. Although the XRD pattern for the decomposition product exhibits the main diffraction peaks for the host, the peaks are broad and asymmetric, which suggests that the lattice undergoes significant changes that partially collapse the structure in poorly crystalline phases. © 1998 Academic Press

Key Words: **misfit layer chalcogenides; exfoliation; polymer intercalation; nanostructures.**

INTRODUCTION

The insertion of organic polymers between layers of an inorganic matrix has promoted intense research activity for two main reasons (1, 2). First, it is an attractive method for preparing new organic/inorganic nanocomposites. Second, these novel materials can improve specific properties (e.g., mechanical, electrical, optical) of the parent components, thus extending the number of potential applications of the individual components. The most familiar polymer intercalated into layered systems is PEO, a water-soluble polymer with a simple structure. The layered inorganic hosts studied, so far include montmorillonite (3), MoS_2 (4a), TiS_2 (4b, 5), MoO_3 (6), $MnPS_3$ (7), $CuFeS_2$ (8), and V_2O_5 (9). The usual preparation strategy, particularly with layered chalcogenides, involves exfoliation of the inorganic matrix, (usually by reacting the lithium-intercalated chalcogenide with water(10)), followed by restacking of the layers in the presence of the organic polymer.

Over this decade, a new family of composite layered chalcogenides of $(MX)_{1+y}(TX_2)_2$ (M = Sn, Pb, Bi, Ln; T = Ti, V, Cr, Mn, Nb; X = S, Se) stoichiometry has been synthesized and characterized (11). Their structures, well documented for $(PbS)_{1.14}(NbS_2)_2$, $(PbS)_{1.18}(TiS_2)_2$, and $(PbSe)_{1.12}(NbSe_2)_2$ from X-ray single crystal measurements, consist of a double layer MX and two TX_2 sandwiches stacked along the c-axis. The TX_2 sandwich has an atomic arrangement similar to that found in binary TX_2 layer compounds, but its lattice symmetry is different from that of the MX slab. This divergence in periodicity makes these materials incommesurate in one direction (the a axis).

A relevant structural property of this family of compounds concerning the intercalation reactions is the formation of an interlayer region defined at the interface of two consecutive close packed chalcogen layers. This gives rises to vacant sites that can be occupied by atomic or molecular intercalants. In this context, lithium, sodium, *n*-alkylamines, alkyldiamines, and cobaltocene can be easily and successfully intercalated (12).

In this paper, we examine the ability of these complex structures to generate nanocomposites with organic polymers, using the methodology for preparation of nanocomposites of binary layered chalcogenides. In fact, chemical exfolation of $(PbS)_{1.12}(NbS_2)_2$ was previously achieved (13) by first intercalating the sulfide with sodium and then exposing the intercalated compound to excess 0.1 N HCl. For this study, we chose $(PbS)_{1.18}(TiS_2)_2$ as the host, which proved the best candidate for intercalation reactions (12).

EXPERIMENTAL

Polycrystalline samples of $(PbS)_{1.18}(TiS_2)_2$ were prepared by heating mixtures of the constituent elements (supplied by Strem Chem.) at an appropriate ratio in evacuated silica tubes. The mixtures were first heated at 300°C for 1 day and then at 900°C for 1 week. The material thus obtained was in the form of high-purity platelike microcrystals, as checked from electron and X-ray diffractions. Moreover, it exhibited a metallic luster, consistent with its metal-like behaviour

0022-4596/98 $25.00

(11). A similar procedure was applied for the synthesis of TiS_2 but heating the mixture of the elements at 500°C for 1 day and then at 900°C for a week. The product identity was determined by X-ray diffraction.

Lithium insertion was performed in an argon-filled glovebox, using *n*-butyllithium under the following conditions: 600 mg of $(PbS)_{1.18}(TiS_2)_2$ was treated with 4 ml of 1.6 *M* *n*-butyllithium in *n*-hexane at ambient temperature for 3 days. Under these conditions, the lithium content, as determined by back-titration of residual intercalant, suggested a stoichiometry of $Li_{2.14}(PbS)_{1.18}(TiS_2)_2$. Polyethyleneoxide (PEO, Aldrich mw = 100000Da) was used as received. Two nanocomposites of different composition were prepared from PEO aqueous solutions of different concentrations, 0.15 *M* (sample A) and 0.30 *M* (sample B). A volume of 50 ml of each was added to 300 mg of $Li_{2.14}(PbS)_{1.18}(TiS_2)_2$ and the mixture immediately ultrasonicated for 30 min, followed by magnetic stirring for 18 h. Then, the samples, that preserved their black colour but lost their metallic luster, were filtered, washed with distilled water several times to remove LiOH and other soluble solids, and air dried.

Powder X-ray diffraction (XRD) patterns were recorded on a Siemens D5000 diffractometer equipped with a graphite monochromator, using Cu$K\alpha$ radiation. For identification purposes, intensities were collected in steps of 0.04°(θ), at 0.12 s per step. For broadening analysis of the reflection lines, intensities were recorded in the same scan step using 3.6 s per step.

Electron micrographs were obtained on a JEOL 200CX microscope. Samples were dispersed in acetone with the aid of ultrasound and placed on carbon-covered copper grids for examination. IR spectra were recorded on a Bomen MB-100 FTIR system, using KBr pellets containing about 1% of the product. Elemental analyses were conducted on a Fisons CHNS analyzer, and thermogravimetric analyses (TG) were carried out on a Cahn Thermobalance, under argon, using a heating rate of $7°C \cdot min^{-1}$ and a flow rate of $50\ ml \cdot min^{-1}$. Temperature-programmed deintercalation (TPD) measurements were carried out on a quartz reactor coupled to a quadrupole mass spectrometer (Sensorlab VG model), using argon at $50\ ml \cdot min^{-1}$ as the carrier gas.

RESULTS AND DISCUSSION

Organic lithium derivatives such as n-butyllithium readily react with misfit layer sulfides, particularly $(PbS)_{1.18}(TiS_2)_2$, to yield lithium intercalates characterized by an expansion of about 0.5 Å per PbS-TiS_2-TiS_2 repeat unit normal to the slabs of the host structure (12a). Indirect methods (e.g., cointercalation solvent phenomena (14)) have revealed that Li^+ ions occupy interstitial sites defined at the TiS_2-TiS_2 interface (one octahedral site and two tetrahedral ones per formula unit). Under the above described experimental conditions, the lithium content per formula unit is slightly greater than 2. This means that both octahedral and tetrahedral positions are occupied, thus resulting in strong repulsion between Li^+ ions that leads to a quasi-amorphous phase as revealed by XRD (see Fig. 1a). Inmersion of this phase in water produces a violent reaction that releases hydrogen and causes a dramatic decrease in the lithium content (to 0.2 ions per formula). This reaction readily exfoliates the lithium intercalate and probably gives rise to single layer suspensions. We failed to detect any such monolayers because they rapidly restack to form aggregates such as those found in other misfit layer sulfides (13). The XRD pattern for this restacked material is shown in Fig. 1b. Most lines basically coincide with those for the unlithiated compound; those marked with an asterisk belong to hydrated phases (14). The electron diffraction pattern for this sample is typical of a misfit layer compound (15) (Fig. 2a) and is characterized by two sets of spots corresponding to the two sublattices associated with PbS and TiS_2 slabs, which are incommensurate in the *a* direction.

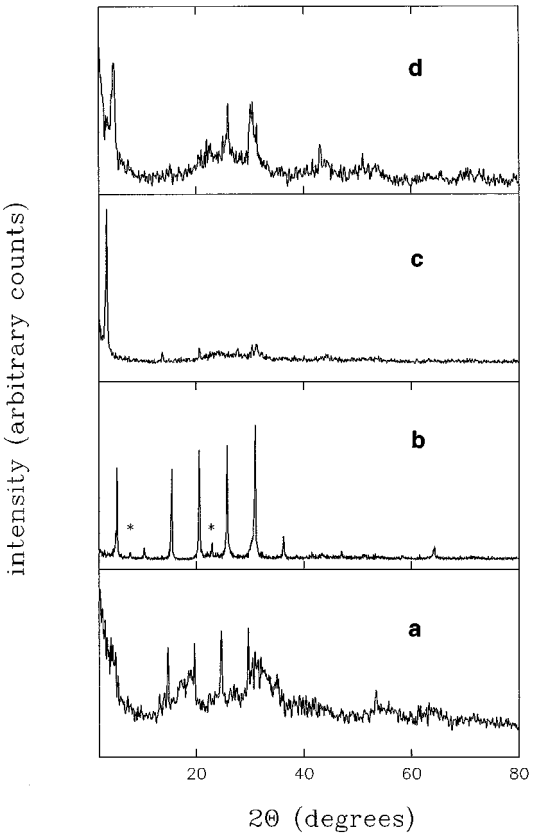

FIG. 1. X-ray diffraction pattern of (a) $Li_{2.14}(PbS)_{1.18}(TiS_2)_2$, (b) $Li_{0.23}(PbS)_{1.18}(TiS_2)_2$, (c) $Li_{0.15}(PEO)_{1.14}(PbS)_{1.18}(TiS_2)_2 \cdot 0.56H_2O$, and (d) $Li_{0.25}(PEO)_{1.79}(PbS)_{1.18}(TiS_2)_2 \cdot 0.88H_2O$ heated at 450°C. (*) Hydrated phase.

A significant structural change is observed when flocculation takes place in the presence of the polymer. Figure 1c

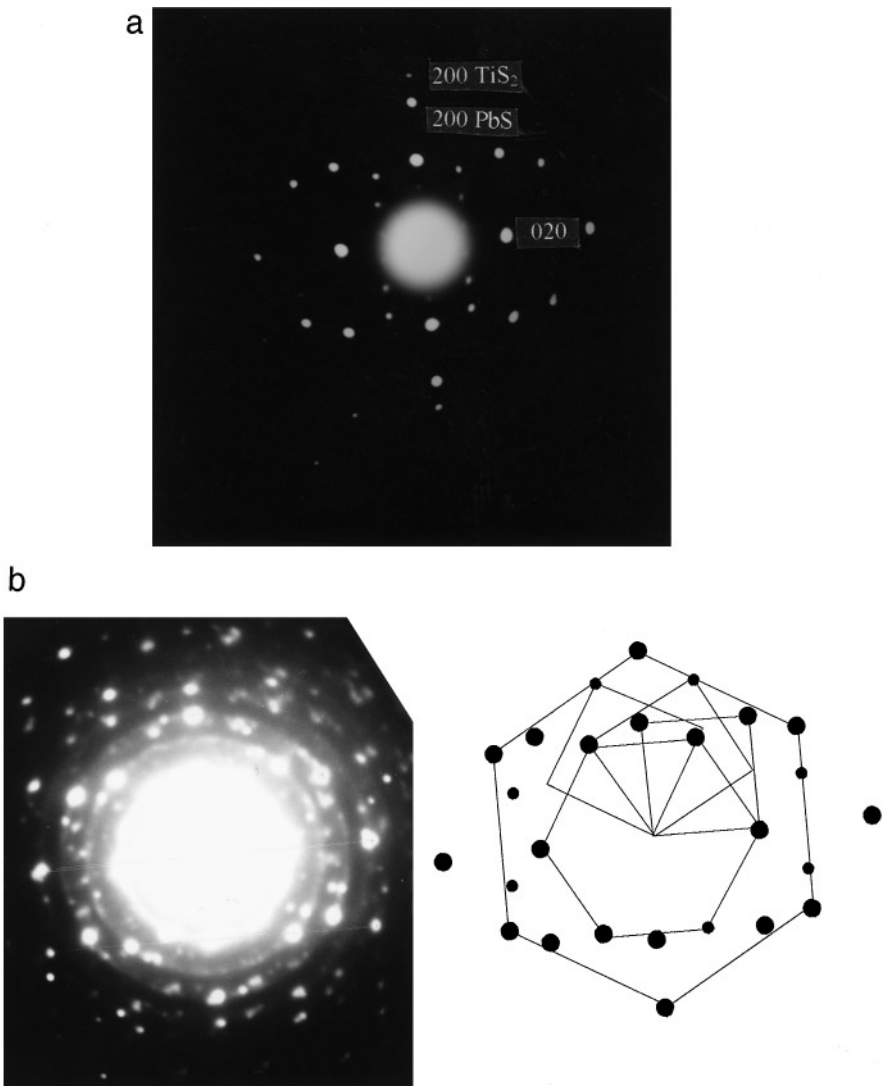

FIG. 2. Electron diffraction pattern of (a) $Li_{0.23}(PbS)_{1.18}(TiS_2)_2$ and (b) $Li_{0.25}(PEO)_{1.79}(PbS)_{1.18}(TiS_2)_2 \cdot 0.88H_2O$.

shows the XRD pattern for the restacked material (sample B). The most salient feature is the presence of a prominent peak at 3.47° (2θ), together with several harmonics of low intensity that are commonly found for other PEO nanocomposites (4). The average basal spacing was 25.70 Å (about 8.4 Å greater than that of the pristine compound). The XRD pattern for sample A is similar to that for sample B; however, the peaks in the former are somewhat less intense. The expansion calculated coincides with that reported for a PEO/TiS_2 nanocomposite prepared either by using N-methylformamide as solvent (5) or a solution of PEO with lithium perclorate in acetonitrile (4b). We failed to obtain any PEO/TiS_2 nanocomposites under the same experimental conditions used for the ternary sulfide. We have no clear explanation for the smaller tendency of TiS_2 to intercalate PEO in comparison with the ternary sulfide. Particle size as a factor for this differential behavior can be discarded since particle size of TiS_2, as revealed by SEM, is smaller than that of $(PbS)_{1.18}(TiS_2)_2$. The smaller ability of TiS_2 to yield nanocomposites with PEO could be due to the difficulty in preparing highly stoichimetric TiS_2. In our case, the real composition of the sample used, as determined from thermogravimetric measurements, was $Ti_{1.028}S_2$. This means that the Ti excess should probably occupy the interstitial positions located at the van der Waals gaps, thus affecting the same positions available for the guest species. On the contrary, the ternary sulfide seems to have completely empty the van der Waals positions defined at the TiS_2-TiS_2 interface. Direct evidence is deduced from accurate X-ray single crystal structure determinations of Ti-based bilayer compounds, e.g. $(PbS)_{1.18}(TiS_2)_2$ (16) and $(SbS)_{1.15}(TiS_2)_2$ (17). These studies have

TABLE 1
Chemical Composition of Original Misfit and the PEO Nanocomposites

Formula	%Li[a]	%C	%H	%S
$Li_{0.23}(PbS)_{1.18}(TiS_2)_2$	0.32(0.32)	–	–	30.3(32.8)
$Li_{0.15}(PEO)_{1.14}(PbS)_{1.18}(TiS_2)_2 \cdot 0.56H_2O$	0.19(0.18)	4.82(4.82)	1.00(1.00)	26.5(29.2)
$Li_{0.25}(PEO)_{1.79}(PbS)_{1.18}(TiS_2)_2 \cdot 0.88H_2O$	0.29(0.29)	7.12(7.13)	1.48(1.48)	25.9(27.5)

[a] Calculated values are shown in brackets.

demonstrated the absence of Ti self intercalated at the TiS_2-TiS_2 interface.

The chemical compositions of exfoliated and restacked samples are shown in Table 1. As in the case of the lithium intercalate treated with water, most Li^+ ions are extracted on flocculation in the presence of PEO. As the PEO concentration increases, so does the polymer content in the host, with little effect on interlayer expansion, however. These composition values can be matched with the corresponding PEO-Li/TiS_2compounds (4b,5). The nanocomposites were obtained as hydrated phases and the sulfur content tended to decrease slightly in the different process,undergone by the host. Changes in surface composition were detected in the course of *in situ* XPS experiments of alkyldiamine deposition from the gas phase (18). We have no direct evidence of the location of water molecules. Although, as shown below, thermogravimetric data, suggest that part of this water is strongly adsorbed in the lattice, the expanded interlayer remains unchanged if the water is removed by heating. The basal space increase found is thus promoted by the polymer intercalation and resembles to that reported in clays (3), MPS_3 (M = Mn, Ni, Fe, Cd) (7) and MS_2 (M = Mo, Ti) (4,5). The interlayer expansion can be interpreted according to two intercalation models: by preserving the polymer helical conformation or by assuming bilayers of PEO between successive TiS_2 sheets in a zigzag conformation. Unfortunately, we could not apply the model recently used by Liu *et al.* (9b), based on the evaluation of one-dimensional electron-density projections on the *c*-axis, owing to the limited number of (001) reflexions and the small value of the peak intensity to background ratio for most peaks. However, complementary information was supplied by IR spectroscopy, despite the poor resolution of the absorption peaks resulting from the high absorbance of the sample. Figure 3 shows the IR spectra for pure and intercalated PEO. The broad, strong band centered at 2890 cm^{-1} in bulk PEO, associated with CH_2 stretching modes, appears in the intercalate form as two well-defined bands at 2855 band 2924 cm^{-1} . This behaviour is commonly found in other PEO nanocomposites and has been ascribed to interactions between oxygen atoms in PEO and interlayer cations (6). The multiple peaks observed in the 1500–800 cm^{-1} region for pure PEO are ill-defined in intercalated PEO

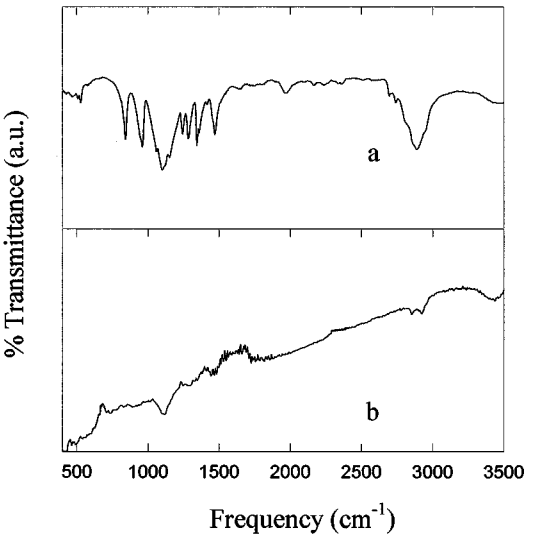

FIG. 3. FT-IR spectra: (a) bulk PEO and (b) $Li_{0.25}(PEO)_{1.79}(PbS)_{1.18}(TiS_2)_2 \cdot 0.88H_2O$.

(only the strong peak centered at 1100 cm^{-1}, which corresponds to C-O stretching, is clearly observed). Its position remains virtually unchanged relative to bulk PEO. A significant feature is the absence of an intense band located about 1300 cm^{-1} which is characteristic of vibrations of O-$(CH_2)_2$-O groups in type I PEO-$HgCl_2$ complexes (19) but is absent in the helical conformation of PEO. The presence of water was confirmed by a broad band centered at 3450 cm^{-1}. A schematic model by assuming a helical conformation of PEO is depicted in Fig. 4. Although to confirm its validity one needs further structural investigations, an alternative model with monolayers of PEO between both TiS_2-TiS_2 and TiS_2-PbS interfaces is unlikely. In fact, the compound $(PbS)_{1.18}TiS_2$, which possesses a PbS-TiS_2-PbS-TiS_2 stacking sequence and contains PbS-TiS_2 interfaces only, intercalates very little lithium (11a). For this reason, chemical delamination, as with $(PbS)_{1.18}(TiS_2)_2$, is unfavorable.

In addition to the position changes in the diffraction peaks observed upon intercalation, the rather sharp original lines for the pristine compound broaden, thus suggesting the formation of smaller crystallites and/or an increase in elastic strains in the host. In order to quantify the microstructural changes induced by polymer intercalation, (001) profiles were analysed using the integral breadth method (20) for separating size and strain broadening. The analysis was based on

$$(\delta 2\theta)\cos^2(\theta) = 16\langle e^2\rangle \sin^2(\theta) + K^2\lambda^2/L^2, \qquad [1]$$

where $(\delta 2\theta)$ is the integral breadth after correction for the instrumental broadening obtained from highly crystalline sillicon powder, $\langle e^2\rangle$ denotes local strains (defined as

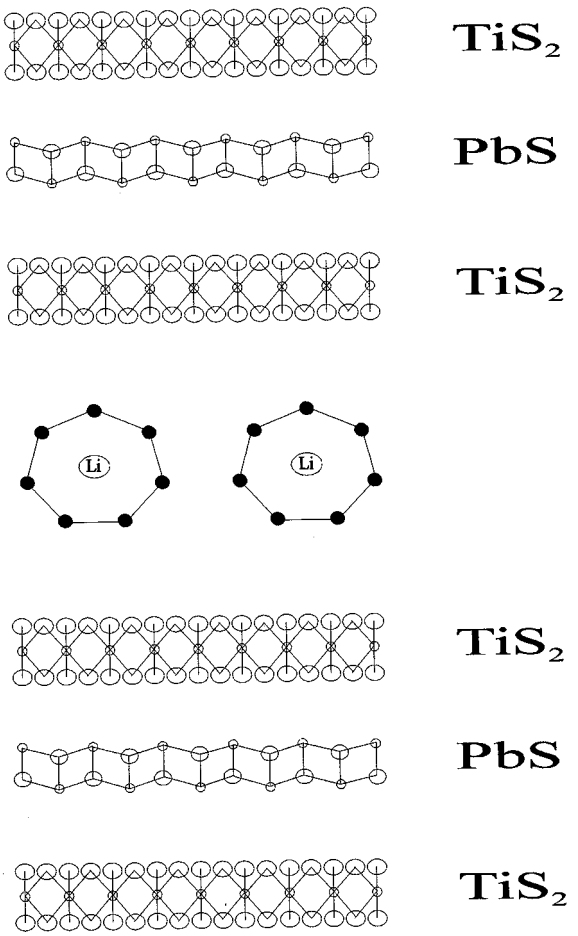

FIG. 4. Schematic projection along [100] for the nanocomposite $Li_{0.25}(PEO)_{1.79}(PbS)_{1.18}(TiS_2)_2 \cdot 0.88H_2O$.

$\Delta d/d$, d being the interplanar spacing), L is crystallite size, and K is a near-unity constant related to crystallite size. The slope, $16\langle e^2\rangle$, and intercept, $K^2\lambda^2/L^2$, were used to determine the distortion and size parameters. Figure 5 shows plots for different reflections of water-treated and polymer-intercalated samples. The crystallite sizes and strains calculated from these plots are collected in Table 2. The results suggest that the stacking coherence length is reduced in the exfolation/adsorption process and that the microstrain content increases significantly by effect of the expansion required to accommodate the polymer into the galleries.

Transmission electron micrographs provided additional evidence of these microstructural changes. They revealed aggregates more densely populated than the polymer-untreated material. This precluded the possibility of obtaining electron diffraction patterns for single microcrystals such as that of Fig. 2a. One common feature was the presence of Debye–Scherrer rings, consistent with the reduced crystallite size and suggestive of random restacking in the monolayers (13). Occasionally, it is possible to differentiate

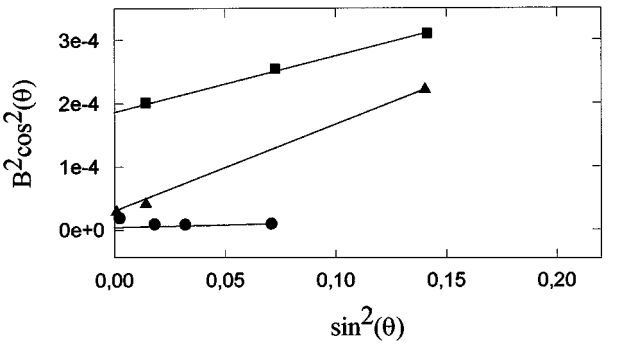

FIG. 5. Plot of Eq. [1] for different [001] reflections: ●, $Li_{0.23}(PbS)_{1.18}(TiS_2)_2$; ■, $Li_{0.15}(PEO)_{1.14}(PbS)_{1.18}(TiS_2)_2 \cdot 0.56H_2O$; ▲, $Li_{0.25}(PEO)_{1.79}(PbS)_{1.18}(TiS_2)_2 \cdot 0.88H_2O$.

in densely spotted micrographs resulting from microcrystal agglomeration, distinct spots due to different orientational variants both of PbS and TiS_2 sublattices (see Fig. 2b). This feature has been associated with the degree of deformation of the sublattices and orientation changes in MX_2 and/or MX layers have been reported in distorted regions of misfit layer compounds (14) and in their lithiated phases (21).

The stability of the intercalates was examined from both thermogravimetric and the mass spectrometric results for desorbed molecules. The temperature range studied was 30–450°C and the following fragments were recorded to detect the polymer release in the mass spectrum: $CH_2{-}CH_2O^+$ (44), $CH_2{-}CH_2^+$(28), O^+ (16), CH_2^+ (14). The mass of first two fragments are coincident with those of CO_2^+ and CO^+, respectively. Moreover, the release of H_2S is frequently observed in thermal deintercalation studies of layer chalcogenides intercalated with organic molecules (12c, 22). For this reason, the base peak for H_2S was also recorded. Unfortunately, the H_2O spectrum could not be recorded, owing to the water background in the experimental system. Figure 6 shows selected TPD curves for sample B. All the above fragments were clearly detected and the formation of CH_2^+ and CH_2O^+ fragments provides direct evidence of polymer volatilization rather than pyrolisis (otherwise unfavourable under these conditions).

TABLE 2
Basal Spacing, Crystallite Size, and Microstrains of PEO Nanocomposites

Sample/Formula	c(Å)	L(Å)	$\langle e^2\rangle \cdot 10^{-3}$
$(PbS)_{1.18}(TiS_2)_2$	17.40	1363	0.036
$Li_{0.23}(PbS)_{1.18}(TiS_2)_2$	17.35(23.01)[a]	516	8.1
A/$Li_{0.15}(PEO)_{1.14}(PbS)_{1.18}(TiS_2)_2 \cdot 0.56H_2O$	25.86	112	534
B/$Li_{0.25}(PEO)_{1.79}(PbS)_{1.18}(TiS_2)_2 \cdot 0.88H_2O$	25.81	284	486

Note. The values for $(PbS)_{1.18}(TiS_2)_2$ and $Li_{0.23}(PbS)_{1.18}(TiS_2)_2$ are included for comparison.

[a] Hydrated phase.

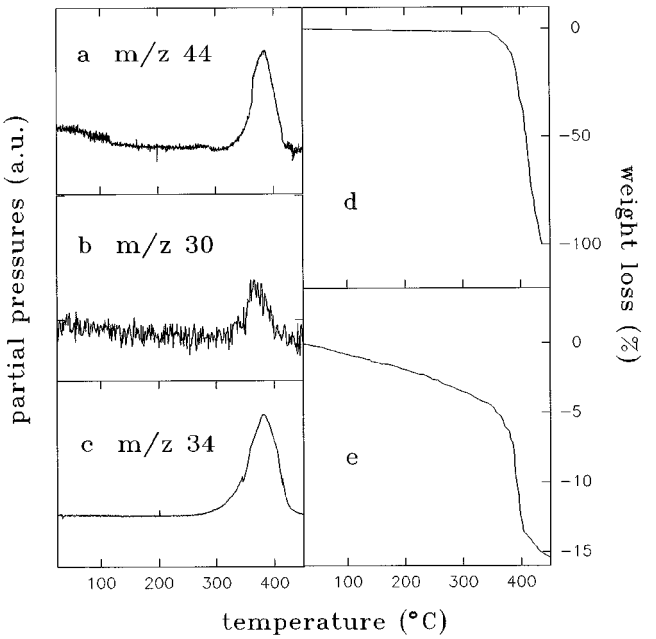

FIG. 6. Thermal analysis of $Li_{0.25}(PEO)_{1.79}(PbS)_{1.18}(TiS_2)_2{\cdot}0.88H_2O$: (a, b, c) temperature-programmed deintercalation spectra of different fragments; (d) TG curve (TG curve of bulk PEO (e) is included for comparison).

TPD profiles exhibited a rather symmetric single peak centered at 370°C suggestive of the presence of one type of polymer species within the layers. The deintercalation temperature was more than 100°C higher than that observed for the release of intercalated amine molecules in the same host (12c). One factor that might account for this unusual thermal stability is polymer/Li^+ interactions. In fact, in the $(PEO)_{0.40}$ $[Na(H_2O)_n]$ MoO_3 nanocomposite, this type of interaction has been demonstrated in ^{23}Na MAS NRM studies (6); also, the thermal decomposition reaches temperatures as high as 400°C.

Although we lack direct evidence for the proton source for the formation of H_2S, H_2O is probably the best candidate. In order to further investigate the origin of this compound, a TG curve was obtained under the same experimental conditions as the TPD curves. Figure 6 shows the results of TG experiments carried out from room temperature to 450°C. Two main features distinguish the TG curves of bulk and intercalated PEO. First, the volatilization temperature for the polymer decreases slightly when the molecules are captured within the galleries of the host matrix. The total weight loss observed for the intercalate was 15.4%, in acceptable agreement with the PEO and water content (15.7%) determined by elemental analysis. This means that the amount of H_2S released is hardly perceptible by weight loss measurements, so one only needs water traces to account for its formation. The second difference is the continuous weight loss undergone by the intercalate from rather low temperatures up to 290°C, which, judging by the wide temperature range observed, presumably corresponds largely to different types of water bound to the lattice. The fact that the formation of H_2S is anticipated about 50°C to the polymer deintercalation temperature favors a direct attack of water molecules on the lattice to release of H_2S:

$$H_2O + S^{2-}_{(lattice)} \rightarrow H_2S + O^{2-}_{(lattice)}. \qquad [2]$$

This reaction is favored by the polymer release, probably because of the lattice rearrangement induced by the deintercalation process. The XRD pattern of the product obtained after the TG experiments showed that the lattice was indeed heavily distorted (Fig. 1d). The diffraction peaks were broad and rather asymmetric, thus indicating that removal of the polymer may also result in partial decomposition of the host.

In conclusion, lithium derivatives of $(PbS)_{1.18}(TiS_2)_2$, which are complex layer sulfides, readily intercalate PEO by treatment of the polymer in an aqueous solution. This is the first reported evidence of the usefulness of exfoliation and flocculation methodology for preparing organic/inorganic nanocomposites of composite layer structure such as misfit layer chalcogenides. This new class of nanocomposite is quite stable; the study of its electronic properties may help answer some questions about this incommensurate structure (particularly the nature of the chemical bonds between MX and TX_2 slabs, which is at the origin of its stability).

ACKNOWLEDGMENTS

The authors express their gratitude to Spain's CICYT (Project PB95-0561) and to the Junta de Andalucía (Group FQM0175) for financial support. The assistance of the Servicio de Espectrometría de Masas and Microscopía Electrónica is also gratefully acknowledged.

REFERENCES

1. R. Schöllhorn, *Chem. Mater.* **8,** 1747 (1996).
2. E. Ruiz-Hitky and P. Aranda, *Anal. Quím.* **93,** 197 (1997).
3. E. Ruiz-Hitky, *Adv. Mater.* **5,** 334 (1993).
4a. R. Bissesur, M. G. Kanatzidis, J. L. Schindler, and C. R. Kannewurf, *J. Chem. Soc. Chem. Commun*, 1582 (1993).
4b. E. Ruiz-Hitky, R. Jiménez, B. Casal, V. Manríquez, A. Santa Ana, and G. González, *Adv. Mater.* **5,** 738 (1993).
4c. J. P. Lemmon and M. Lerner, *Chem. Mater.* **6,** 207 (1994).
4d. G. González, M. A. Santa Ana, and E. Benavente, *J. Phys. Chem. Solids* **58,** 1457 (1997).
5. J. P. Lemmon, W. Jinghe, C. Onakhi and M. M. Lerner, *Electrochim. Acta* **40,** 2245 (1995).
6. L. F. Nazar, H. Wu and W. P. Power, *J. Mater. Chem.* **5,** 1985 (1995).
7a. I. Lagadic, A. Leaustic, and R. Clément, *J. Chem. Soc., Chem. Commun.*, **1396** (1992).
7b. C. O. Onakhi and M. M. Lerner, *Chem. Mater.* **8,** 2016 (1996).
8. C. Múgica, R. Durán, J. Llanos and R. Clavijo, *Mat. Res. Bull.* **31,** 483 (1996).

9a. Y. J. Liu, D. C. De Groot, J. L. Schindler, C. R. Kannewurf, and M. G. Kanatzidis, *Chem. Mater.* **3,** 392 (1991).
9b. Y. J. Liu, J. L. Schindler, D. C. De Groot, C. R. Kahnewurf, W. Hirpo, and M. G. Kanatzidis, *Chem. Mater.* **8,** 525 (1996).
10. W. R. Divigalpitiya, R. R. Frindt, and S. R. Morrison, *Science* **246,** 369 (1989).
11. G. A. Wiegers, *Prog. Solid State Chem.* **24,** 1 (1996) and references therein.
12a. L. Hernán, P. Lavela, J. Morales, J. Pattanayak, and J. L. Tirado, *Mat. Res. Bull.* **26,** 1211 (1991).
12b. L. Hernán, J. Morales, L. Sánchez, and J. L. Tirado, *Solid State Ionics* **58,** 179 (1992).
12c. L. Hernán, P. Lavela, J. Morales, L. Sánchez, and J. L. Tirado, *J. Mater. Chem.* **6,** 861 (1996).
12d. L. Hernán, J. Morales, L. Sánchez, J. L. Tirado, J. P. Espinós, and A. R. González-Elipe, *Chem. Mater.* **7,** 1576 (1995).
13. P. Bonneau, J. L. Mansot, and J. Rouxel, *Mat. Res. Bull.* **28,** 757 (1993).
14. P. Lavela, J. Morales, and J. L. Tirado, *Chem. Mater.* **4,** 2 (1992). [P. Lavela, J. Morales, and J. L. Tirado, *J. Solid State Chem.* **124,** 238 (1996)].
15. S. Kuypers, J. Van Landuyt, and S. Amelinckx, *J. Solid State Chem.* **86,** 212 (1990).
16. C. Auriel, A. Meerschaut, R. Roesky, and J. Rouxel, *Eur. J. Solid State Inorg. Chem.* **29,** 557 (1992).
17. Y. Ren, A. Meetsma, V. Petricek, S. van Smaalen, and G. A. Wiegers, *Acta Cryst.* **B 51,** 275 (1995).
18. J. Santos, unpublished results.
19. R. Iwamoto, Y. Saito, H. Ishihara, and H. Tadokoro, *J. Polymer. Sci.* **6,** 1509 (1968).
20. H. P. Klug and L. E. Alexander, "X-ray Diffraction Procedures for Polycrystalline and Amorphous Materials," p. 661, Wiley, New York, 1974.
21. L. Hernán, J. Morales, J. Pattanayak, and J. L. Tirado, *J. Solid State Chem.* **100,** 262 (1992).
22. P. A. Joy and S. Vasudevan, *J. Amer. Chem. Soc.* **114,** 7792 (1992). [P. A. Joy and S. Vasudevan, *Chem. Mater.* **5,** 1182 (1993)].